ARTICLE

Effect of Solvent and Subsequent Thermal Annealing on the Performance of Phenylenevinylene Copolymer:PCBM Solar Cells

G. D. Sharma,*,†,‡ P. Suresh,† S. S. Sharma,§ Y. K. Vijay,§ and John A. Mikroyannidis*,||

Physics Department, Molecular Electronic and Optoelectronic Device Laboratory, Jai Narain Vyas University, Jodhpur (Raj.) 342005, India, Jaipur Engineering College, Kukas, Jaipur (Raj.), India, Thin film & Membrane Science Laboratory, Department of Physics, University of Rajasthan, Jaipur (Raj.) 302004, India, and Chemical Technology Laboratory, Department of Chemistry, University of Patras, GR-26500 Patras, Greece

ABSTRACT The morphology of the photoactive layer used in the bulk heterojunction photovoltaic devices is crucial for efficient charge generation and their collection at the electrodes. We investigated the solvent vapor annealing and thermal annealing effect of an alternating phenylenevinylene copolymer **P**:PCBM blend on its morphology and optical properties. The UV−visible absorption spectroscopy shows that both solvent and thermal annealing can result in self-assembling of copolymer **P** to form an ordered structure, leading to enhanced absorption in the red region and hole transport enhancement. By combining the solvent and thermal annealing of the devices, the power conversion efficiency is improved. This feature was attributed to the fact that the PCBM molecules begin to diffuse into aggregates and together with the ordered copolymer **P** phase form bicontinuous pathways in the entire layer for efficient charge separation and transport. Furthermore, the measured photocurrent also suggests that the space charges no longer limit the values of the short circuit current (J_{sc}) and fill factor (FF) for solvent-treated and thermally annealed devices. These results indicate that the higher J_{sc} and PCE for the solvent-treated and thermally annealed devices can be attributed to the phase separation of active layers, which leads to a balanced carrier mobility. The overall PCE of the device based on the combination of solvent annealing and thermal annealing is about 3.7 %.

KEYWORDS: phenylenevinylene copolymer • solvent and thermal annealing • bulk heterojunction solar cells

INTRODUCTION

In recent years, solar cells based on conjugated polymers have attracted considerable attention because of their potential for low-cost, light-weight, good compatibility with the roll-to-roll process for making flexible large-area devices (1−5). Efficient organic solar cells (OSCs) use an active layer of bulk heterojunction (BHJ), which consists of a phase-separated blend of organic donor and acceptor components, where a conjugated polymer is often used as electron donor and a fullerene derivate as electron acceptor unit. By an intimate mixing of the electron donor and acceptor materials, the intrinsic limitations related to low mobility and life time of excitons in organic semiconductors can be overcome, resulting in effective carrier generation at the extended donor−acceptor (D−A) interface. Currently, poly(3-hexylthiophene) (P3HT) has proved to be one of the most promising donors and the PCE of OCSs based on its thin film blend with [6,6]-pheny-C61 butyric acid methyl ester (PC_{61} BM) has reached approximately 4−5 % (6−9). However, it is difficult to further improve the efficiency of OCSs based on P3HT because of the relatively large band gap (~2.0 eV) of P3HT, which limits the absorption of near infrared light and thus lowers the light harvesting and efficiency of the devices. The relatively small energy level onset between its highest occupied molecular orbital (HOMO) and the lowest unoccupied molecular orbital (LUMO) of PCBM limits the value of J_{sc} and open circuit voltage (V_{oc}) (10).

One of the fundamental features that limits the efficiency in OCSs is the band gap of conjugated polymer. The control over the band gap is necessary while designing new materials. This band gap engineering allows designing and synthesizing new materials with maximum overlap of absorption spectrum with the solar emission spectrum. It is often found that the synthesis of a low band gap polymer is not the only solution to address this problem but also the position of the HOMO and LUMO levels limits the V_{oc} of the photovoltaic (PV) cell (11, 12). These two properties of organic materials can be controlled by introducing alternating electron-donating and electron-accepting units in the polymer backbone. Theoretical and experimental research works in OSCs have demonstrated that such D−A type polymers have great potential as a class of promising

* Corresponding author. Tel: 91-0291-2720857 (G.D.S.); +30 2610 997115 (J.A.M.). Fax: 91-0291-2720856 (G.D.S.); +30 2610 997118 (J.A.M.). E-mail: sharmagd_in@yahoo.com (G.D.S.); mikroyan@chemistry.upatras.gr (J.A.M.).
Received for review October 23, 2009 and accepted December 29, 2009
† Jai Narain Vyas University.
‡ Jaipur Engineering College.
§ University of Rajasthan.
|| University of Patras.
DOI: 10.1021/am900728f

Published on Web 01/12/2010

materials for OSCs (13, 14). It has been reported that the conjugated D and A units combined through π-conjugated linkers have an intrinsic intramolecular charge transfer (ICT) character, reduce the optical band gap, and allow the absorption of the molecule to match well with the solar spectrum (15). Moreover, by flexible selection or modification of the D and A functional groups, desirable thermal properties, electronic structures, photoelectric properties, and solubility may be achieved (16). Using this approach, several narrow band gap D−A type conjugated polymers have shown promising performances with PCE of ~3−6% (17−21). However, in these linear D−A copolymers, the molecular interactions and packing orientation of the conjugating moieties need to be carefully controlled to ensure proper processability and charge transporting properties (5, 22). Moreover, moieties that can support quinoidal structure lead to narrow polymer band gap, which is crucial to efficiently harvesting solar energy (23).

Several other methods have been adopted to improve the PCE of solar cells using polymer:PCBM blend active layer (7, 24). Thermal annealing of the active layer can enhance the light absorption properties and the hole mobility by inducing the self organization of conjugated polymers (7, 12, 25). However, the exciton loss also increases when the domain size of donor or acceptor phase exceeds the exciton diffusion length of conjugated polymers (26). Therefore, the optimization of thermal annealing temperature and time is needed to achieve the maximum PCE (27). Similarly, the solvent annealing of conjugated polymer:PCBM thin film can also enhance the performance of the solar cells (6, 28). Nevertheless, the effect of solvent annealing on the PCE of polymer solar cells has not been fully understood in the case of copolymer:PCBM. To obtain high performance of the copolymer:PCBM solar cells, an appropriate solvent annealing process that leads to a desirable nanophase separation is needed.

Recently, many studies have been published considering the fabrication methods for producing solar cells with higher flexibility, which has been a field of continuous research (29−31). However, the stability and lifetime of the polymer solar cells are factors that must be seriously taken into account. There have been a considerable number of publications regarding this particular subject (32−37).

Herein, we demonstrate an approach for enhancing the PV performance of the polymer solar cells based on a D−A phenylenevinylene copolymer **P**:PCBM blend, by treating the active layer with dichlorobenzene (DCB) vapor and subsequently thermal annealing. Compared to the device (without solvent annealing) that is subjected only to thermal annealing, the DCB vapor treatment can induce copolymer **P** self organizing into ordered structure, resulting in enhanced absorption in visible region and hole mobility. The subsequent thermal annealing of the device at 120 °C makes PCBM molecules diffuse into aggregates, which when combined with the ordered copolymer phase form bicontinuous pathways in the entire active layer for efficient charge separation and transport.

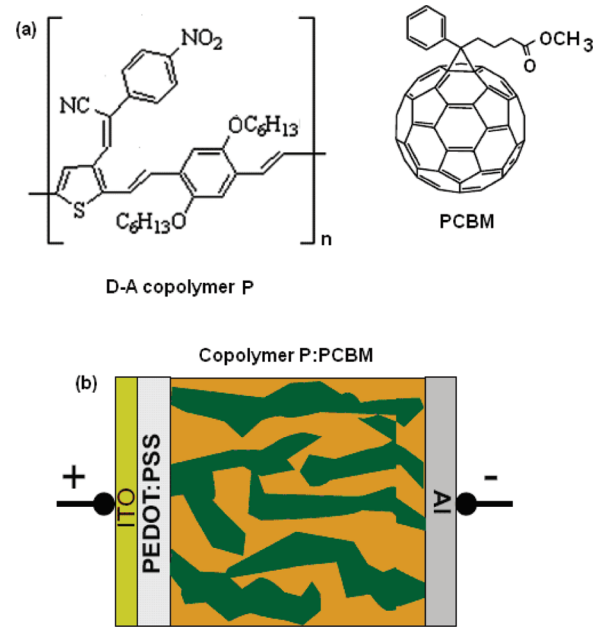

FIGURE 1. (a) Chemical structure of copolymer P and PCBM; (b) device structure.

EXPERIMENTAL SECTION

An alternating *p*-phenylenevinylene copolymer **P** containing thiophene with electron-donating dihexyloxyphenylene and electron-withdrawing cyanovinylene 4-nitrophenyl was synthesized by Heck coupling (38) and used as electron donor with PCBM as electron acceptor. The chemical structure of copolymer **P** and PCBM are shown in Figure 1a. The detailed synthesis and characterization of copolymer **P** has been described in our earlier communication (38). It has been fully characterized by FT-IR and ^{1}H NMR spectroscopy as well as elemental analysis. The preparation yield of **P** after the purification process was 72% and the number average molecular weight (M_n) was 9600, by GPC, with polydispersity of 2.6 (38).

The copolymer **P**:PCBM blend solution (weight ratio 1:1) was prepared in chloroform at a concentration of 10 mg/mL. The devices were fabricated on the top of the indium tin oxide (ITO) coated glass substrates, which had been cleaned by successive ultrasonic treatment in acetone and isopropyl alcohol and then dried at 100 °C for 20 min. After cleaning the ITO substrate, the thin film of PEDOT:PSS was spin coated to layer with a thickness of 50−60 nm and baked at 100 °C for 1 h in an oven. The 80−90 nm thick photoactive layer (**P**:PCBM) was spin coated from the above prepared blend solution on the top of PEDOT:PSS layer for 1 min to minimize the residual solvent. The film thickness was adjusted by controlling the spin rate. The spinning rate to deposit the blend was 1500 rpm and the thickness of the films was about 90−100 nm. The solvent annealing treatments of the **P**:PCBM blend films were carried out before the deposition of the metal electrode. The samples were transferred into a glass jar filled with DCB, where they remained for 30 min. The solvent annealing was controlled by the slow evaporation rate of the solvent, which was carried out by adding a small amount of solvent into the glass jar to keep the film wet until it had completely solidified. Finally, the Al electrodes were thermally deposited on the top of the blend film and the effective area of the devices is about 0.14 cm^2. The thermal annealing was carried out at 120 °C for 1 min on a hot plate in ambient conditions and then cooled down to room temperature. The configuration of the device structure is shown in Figure 1b. We have fabricated the following four devices:

(i) ITO/PEDOT:PSS/copolymer **P**:PCBM/Al (D1)

(ii) ITO/PEDOT:PSS/copolymer **P**:PCBM/Al (thermally annealed) (D2)

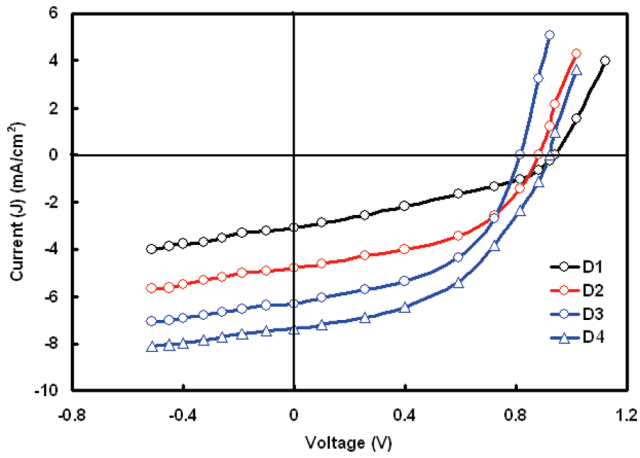

FIGURE 2. Current−voltage characteristics of four devices under white light illumination of intensity 100 mW/cm², as-cast (D1), as-cast annealed (D2), DCB-treated (D3), and thermally annealed DCB-treated (D4).

(iii) ITO/PEDOT:PSS/copolymer **P**:PCBM (solvent annealed)/Al (D3)

(iv) ITO/PEDOT:PSS/copolymer **P**:PCBM (solvent annealed/Al (thermally annealed) (D4)

Current−voltage ($J-V$) characteristics of the devices under white light illumination were measured using a computer-controlled Keithley 236 source meter. A 100 W halogen lamp was used as light source and the illumination intensity was measured with luxmeter calibrated with Si-diode. The illumination intensity was kept constant at 100 mW/cm² for each measurement. The optical absorption of the **P**:PCBM blend films was measured using a Perkin-Elmer 35 UV−visible spectrophotometer on quartz substrates.

The incident photon to current efficiency (IPCE) of the devices was measured by illuminating the device with a halogen lamp using a monochromator and measuring the resulting photocurrent with a Keithley source meter under short-circuit conditions using the following expression

$$\mathrm{IPCE}(\%) = 1240 J_{sc}/\lambda P_{in} \qquad (1)$$

where J_{sc} is the short-circuit photocurrent and λ and P_{in} are the wavelength and illumination intensity of the incident light, respectively.

The crystallinity of the blends was studied using the X-ray diffraction (XRD) technique (panalytical make USA) having CuKα, as radiation source of wavelength $\lambda = 1.5405$ A° with the composite films coated on the quartz substrate.

RESULTS AND DISCUSSION

Figure 2 shows the $J-V$ characteristics of the devices based on various treatments, under white light illumination of 100 mW/cm². The PV parameters of the devices were summarized in Table 1. The PV device without any treatment (device D1) shows an V_{oc} of approximately 0.94 V, J_{sc} of 3.11 mA/cm², and FF of 0.49. The overall PCE of the device is 1.43 %. When this device is annealed at 120 °C for 1 min (device D2), the V_{oc} slightly drops to 0.88 V and the J_{sc} and FF increase to 4.98 mA/cm² and 0.54, respectively. These values lead to an efficiency of 2.37 %. After solvent annealing (DCB-treated active layer) (device D3), the J_{sc} (6.2 mA/cm²) and FF (0.53) increases dramatically, whereas a reduction in V_{oc} (0.82 V) is observed. The increase in J_{sc} compensates for the decrease of the V_{oc}, and leads to an improvement in PCE up to 2.70 %. It can be seen from the $J-V$ curve under illumination, the shunt resistance has been lowered for the device D3, which may result in a decrease in V_{oc}. In the device based on the thermally annealed DCB treated blend (D4), the J_{sc} increased from 6.2 mA/cm² to 7.4 mA/cm², the V_{oc} increased to 0.88 V, and the FF rises to 0.57, leading to an overall PCE of 3.70 %. The V_{oc} value of the device based on the DCB treated active layer drops significantly. It is widely accepted that the energy difference between the HOMO of the donor and the LUMO of the acceptor determines the V_{oc} value of the BHJ OSCs (10).

Table 1. Summary of Photovoltaic Parameters of the Devices Based on Copolymer P:PCBM Blends with Different Annealing Conditions

device	short circuit current (J_{sc}) (mA/cm²) (std. dev)	open circuit voltage (V_{oc}) (V) (std. dev)	fill factor (FF) (std. dev)	power conversion efficiency (η) (%) (std. dev)
D1	3.11 (0.45)	0.94 (0.03)	0.47 (0.02)	1.37 (0.14)
D2	4.80 (0.48)	0.88 (0.02)	0.50 (0.025)	2.20 (0.16)
D3	6.32 (0.53)	0.81 (0.015)	0.55 (0.03)	2.80 (0.20)
D4	7.40 (0.70)	0.88 (0.024)	0.57 (0.04)	3.70 (0.28)

The increase in the PCE of the device upon solvent annealing and the subsequent thermal annealing can be understood in terms of improvement in light absorption, by extending the conjugation length, and balance charge transport, by increasing the hole mobility of copolymer **P**. These results were mainly attributed to the improved crystalline morphology of copolymer **P**, which can easily self organize into well-ordered chains during the solidification from the wet film. The information about the degree of the crystallinity in the conjugated polymer films can be evaluated by investigating the UV−visible absorption spectra in different conditions. We have recorded the UV−visible spectra of the copolymer **P**:PCBM blend treated with DCB (solvent annealing) for different times. It is found that the red shift and vibronic shoulders in the spectra of the copolymer **P**:PCBM blend film increased with the solvent annealing time and became saturated beyond solvent annealing time of 30 min. The absorption spectra of blend film (as cast), treated with DCB for 30 min and thermally annealed DCB treated blend films are shown in Figure 3. For the as-cast film of the copolymer **P**:PCBM blend, the absorption peak is at 630 nm and the absorption onset at 730 nm. In the case of DCB-treated film, the absorption intensity of the UV−visible absorption peak at 640 nm, which is close to the absorption maximum of the copolymer **P** film, increases and three vibronic absorption shoulders are clearly observed, indicating an ordering of copolymer **P** domain. The overall absorption spectra were red shifted after the solvent annealing and thermal annealing. This behavior can be interpreted assuming that the red shifted spectrum results from a lower energy state of the delocalized excitons in the highly π-conjugated copolymer **P** domains, as has been observed in the case of P3HT (39−42). Therefore, the lowering of V_{oc} for device based on DCB treated blend can be explained by the reduced

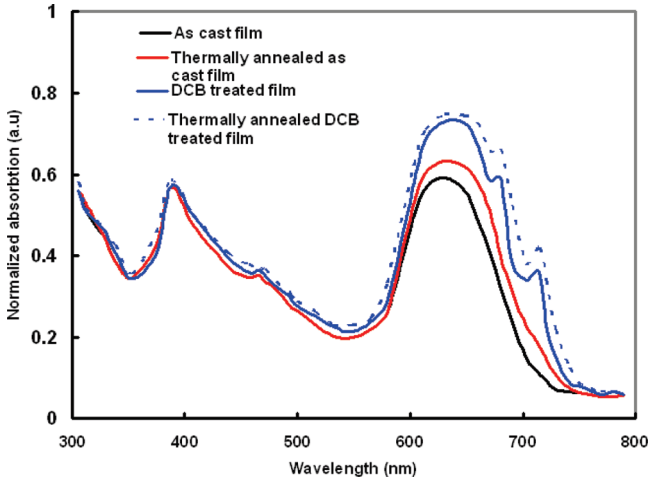

FIGURE 3. UV−visible absorption spectra for copolymer P:PCBM blend films under various conditions of treatment.

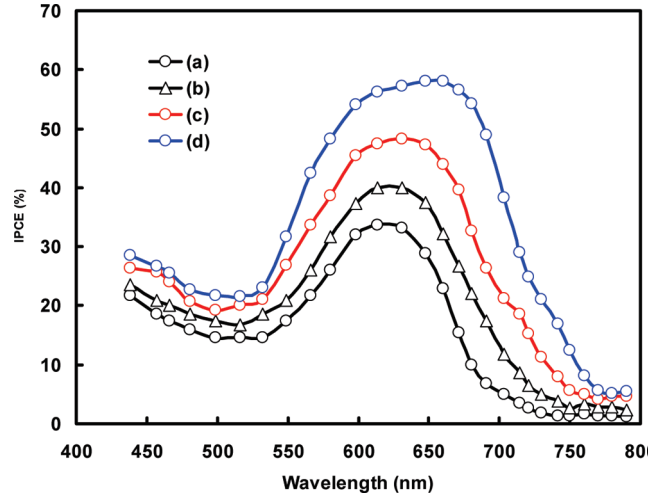

FIGURE 4. IPCE spectra for BHJ devices based on copolymer P:PCBM blend films under various conditions of treatment (a) as-cast, (b) thermally annealed, (c) DCB-treated, and (d) themally annealed DCB-treated blend.

optical band gap of copolymer **P** donor. Compared with the annealed film (before solvent annealing), the absorption of the DCB vapor-treated films are more red shifted and become much stronger in the red region, attributing to an enhanced conjugation length and more ordered structure of copolymer **P**. This indicates that the solvent annealing is a more effective way to realize copolymer **P** self organization. Because the solvent molecules can penetrate into the film and increase the space between polymer chains, the chains become more mobile and self organization can occur to form ordering. It is observed that the absorption of the DCB treated film slightly changes after its thermal annealing. However, the J_{sc} of the device based on the thermally annealed solvent treated blend is significantly higher than the one for the device with only solvent treated blend. This indicates that the enhancement in $J_{sc,}$ is attributed not only to the increase in optical absorption but also to the improved balanced charge transport as well.

The J_{sc} is directly related to the external quantum efficiency (EQE), which is the product of light absorption, exciton diffusion, charge transfer and charge collection efficiency (43−45). Therefore, the increase in the light absorption, in the present devices with different treatments, can not be the main factor for the increase in the J_{sc}. In organic PV devices, the photocurrent generation is governed by a number of sequential processes: the generation of excitons after the absorption of the light by the active layer, followed by the exciton diffusion towards the D−A interface and dissociation via ultra fast charge transfer. After the dissociation, a geminate pair of a hole at the donor and an electron at the acceptor is formed. Because of the low dielectric constant of the organic materials, these electron-hole (e-h) pairs are strongly bound by coulomb interactions with typical energies of several tenths of an electron volt. To generate a photocurrent, these bound e-h pairs must dissociate into free charge carriers and subsequently move to the electrodes before the recombination process takes place.

To get information about the origin of the increase in J_{sc} of the device using different copolymer **P**:PCBM blends, we have measured the IPCE spectra of the devices and we present them in Figure 4. The IPCE spectra of the devices resemble the absorption spectra of the corresponding blend used in the devices. This indicates that the J_{sc} is mainly attributed to the exciton generated because of the absorption of photons in copolymer **P**.

In organic BHJ PV devices, the incident photon to current efficiency (IPCE), is the ratio of the measured photocurrent to the incoming light photons per unit area and time of the device. The IPCE of D/A heterojunction solar cells is represented by the product of the efficiencies of four sequential steps for charge generation (46)

$$\eta_{IPCE} = \eta_A \eta_{ED} \eta_{CT} \eta_{CC} = \eta_A \eta_{IQE} \quad (2)$$

where η_A, $\eta_{ED,}$ η_{CT}, and η_{CC} are the efficiencies of photon absorption to generate an exciton, exciton diffusion to the D−A interface, exciton dissociation by charge transfer, and charge collection at the electrodes, respectively. The internal quantum efficiency (η_{IQE}) depends mainly on the blend morphology of photoactive layer. Therefore, the increase in the IPCE and the J_{sc} upon the solvent and thermal annealing is attributed to the improved light absorption by the photoactive layer and change in the crystallinity of the copolymer in the blend. The latter was observed in the XRD pattern of the blend films under different conditions, which is discussed in one of the following sections of this paper.

After photoinduced electron transfer at the D−A interface, electrons are transferred to PCBM phase, whereas holes remains in the copolymer chain. Subsequently, the free electron and holes must be transported via percolated PCBM and copolymer **P** pathways towards the electrodes to produce the photocurrent. Therefore, the electron transport in PCBM and the hole transport in the copolymer is crucial for the PV performance of the BHJ devices. For pure PCBM, the electron mobility (μ_e= 2.0 × 10^{-3} cm^2/(V s)) is about 250 times higher than the hole mobility in pure copolymer **P** (7.6

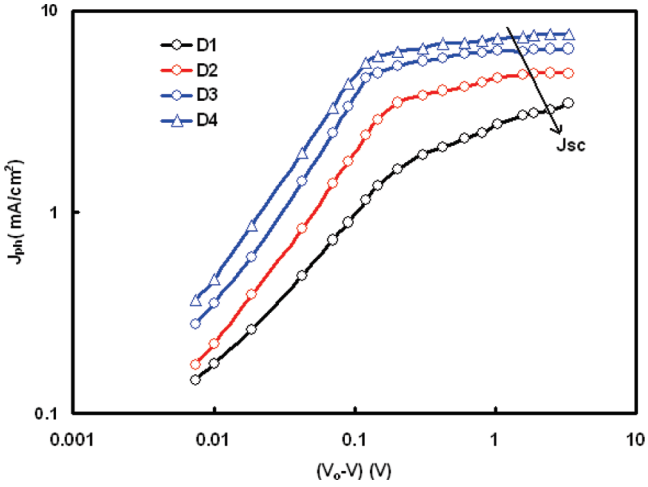

FIGURE 5. Double logarithmic plot of the photocurrent (J_{ph}) as a function of the effective applied voltage ($V_o - V$) for the different devices. The solid line indicates the short circuit current (J_{sc}).

$\times 10^{-6}$ cm^2/(V s)). It has been reported that photocurrent can be determined by field- and temperature-dependent dissociation probability $P(E,T)$, of an e-h pair at the D−A interface (47, 48). Because the exciton dissociation efficiency is almost the same to the probability of e-h pair dissociation, we have compared the P(E,T) values of all devices.

Figure 5 shows the reverse bias dependence of photocurrent (J_{ph}) for devices fabricated with different blends, measured by subtracting the dark $J-V$ characteristics from the respective $J-V$ curves measured under illumination. J_{ph} is plotted as a function of the effective voltage across the device, $V_o - V$, where V_o is the compensation voltage defined as voltage at which $J_{ph} = 0$ (39). In the case of the devices D2, D3, and D4, the photocurrent increases linearly with effective voltages at low voltages and subsequently trends to saturate. The linear behavior at low effective voltages is the result of a direct competition between diffusion and drift currents. In the saturation region for $(V_o - V) > 0.1-0.2$ V, the photocurrent can be approximated by $J_{ph} = qG(E,T)d$, where d is the thickness of the active layer and $G(E,T)$ is the product of $P(E,T)$ and the maximum generation rate of a bound e-h pairs (G_{max}). At high voltage $(V_o - V) > 1$ V, all the e-h pairs are dissociated and the photocurrent is saturated at $J_{sat} = qG_{max}d$. The calculated charge transfer probabilities under short circuit conditions ($P_{sc} = J_{sc}/J_{sat}$) are greater than 0.76 and almost the same for all devices. This indicates that the charge transfer efficiency is not a limiting factor that determines the photocurrent.

We have investigated the charge collection efficiency by measuring the charge carrier mobility in the photoactive layer by means of space charge limited current (SCLC) measurements. We have extracted the hole and electron mobilities from the SCLC $J-V$ characteristics in dark for hole only and electron only devices (42, 49). Figure 6a shows the dark $J-V$ characteristics of ITO/PEDOT:PSS/copolymer **P**:PCBM/Au hole only devices as a function of applied voltage corrected by a built in voltage (difference between the HOMO of copolymer and work function of Au) (49). In the same manner, we have also fabricated the electron only

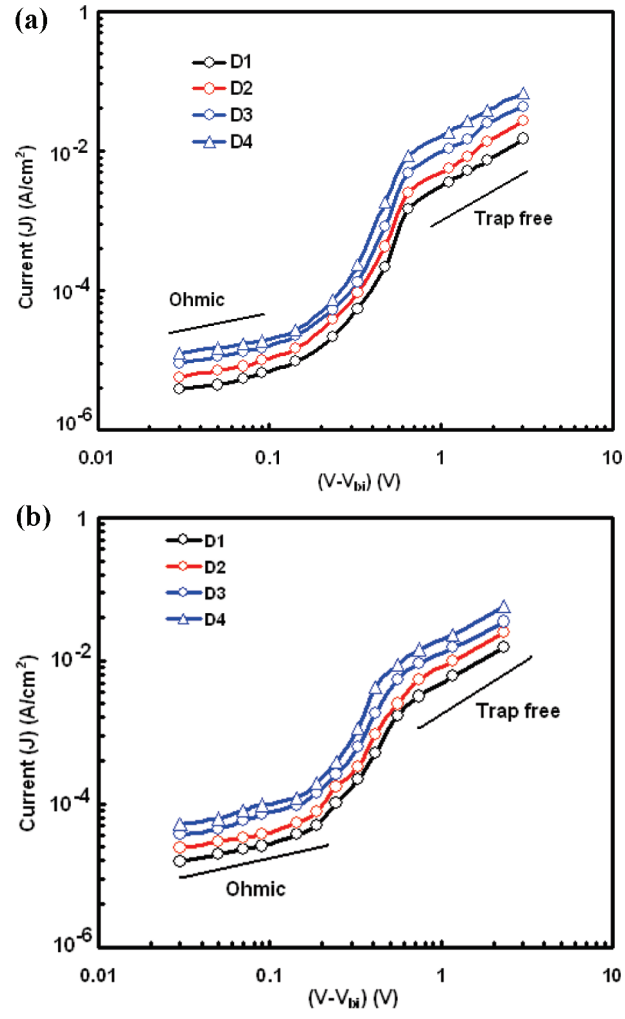

FIGURE 6. (a) Dark current−voltage characteristics for ITO/PEDOT:PSS/copolymer P:PCBM/Au hole-only devices. (b) Dark current−voltage characteristics for Al/copolymer P:PCBM/Al electron-only devices.

devices having structure Al/copolymer **P**:PCBM/Al and investigated the $J-V$ characteristics in dark (Figure 6b). At low voltages, the slope of these curves is about unity, indicating the Ohmic conduction, which is an effect of thermal free carriers. It can be seen from Figure 6a,b that there is a trap-filled limit region in between the Ohmic and trap-free SCLC regions. The SCLC behavior in the trap-free region can be characterized using the Mott−Gurney square law

$$J = (9/8)\varepsilon\mu\left(\frac{V^2}{d^3}\right) \qquad (3)$$

where μ is the mobility of charge carrier, V is the applied voltage corrected for built in voltage, ε is the dielectric constant of the active layer equal to 3.5 as reported for most of the organic materials, and d is the thickness of the layer which is equal to 90 nm for calculation. The electron and hole mobilities in the different active layers estimated using eq 3 and Figure 6a,b are compiled in Table 2. The hole mobility for the thermally annealed active layer is higher than the one for the as-cast active layer, which was attributed

Table 2. Hole and Electron Mobilites of Copolymer P:PCBM Blend Films

film	hole mobility (μ_h) ($cm^2/(V\ s)$)	electron mobility (μ_e) ($cm^2/(V\ s)$)	μ_e/μ_h
as-cast	$9.5. \times 10^{-6}$	7.0×10^{-4}	74
thermally annealed	2.5×10^{-5}	7.8×10^{-4}	31
solvent annealing	4.2×10^{-5}	8.2×10^{-4}	19
combined solvent and thermal annealing	6.7×10^{-5}	8.5×10^{-4}	12

to the self organization of copolymer during thermal annealing. The device based on the DCB vapor-treated blend layer shows higher hole mobility than the annealed active film-based device. This observation indicates more ordered copolymer **P** films formed by the DCB vapor treatment. The hole mobility in copolymer **P**:PCBM film is further enhanced by thermal annealing of the DCB-treated blend, which is almost more than one order of magnitude larger than the as-cast device (D1). The electron mobility has also been improved by the DCB treatment. When the copolymer **P**:PCBM blend film is treated with DCB vapor (D2), the copolymer chain self-organizes into the order structure and at the same time PCBM molecules begin to aggregate for an enhance electron transport. The electron mobility for copolymer **P**:PCBM films with and without DCB vapor treatment is enhanced by thermal annealing. This indicates that the thermal annealing can also effectively activate PCBM molecules to diffuse and aggregate into clusters for better electron transport.

According to the Goodman and Rose model, the $J-V$ characteristics of PV devices can be classified into four regions, namely, linear, transition, half power, and saturation, as the applied field increases (50). However, only half power and saturation regions are possible when hole mobility is considerably lower than electron mobility. On the other hand, only linear and saturation regions are possible when the carrier mobility is perfectly balanced. As can be seen in the device D1, a half power dependence of photocurrent is observed within the full range of applied voltage except for $V_o - V < 0.12$ V. This indicates that the space charges limit the charge collection efficiency and photocurrent. It can be seen in Table 2 that the mobility difference in hole and electron decreased significantly for both devices based on DCB-treated and thermally annealed DCB-treated blend films. This indicates that the space charge effect diminishes for both devices.

Thin film XRD was used to determine the differences in crystallinity of the copolymer **P**:PCBM blended films (as-cast, annealed, DCB-treated, and thermally annealed DCB treated) and the images are shown in Figure 6. The mean crystallite size (L) of the polymer crystallites have been estimated using the well known Scherrer's relation

$$L = \frac{0.9\lambda}{\Delta_{2\theta}\cos\theta} \tag{4}$$

where $\Delta_{2\theta}$ is the full width at half maximum of the peak, λ is radiation source of wavelength $\lambda = 1.5405$ Å.

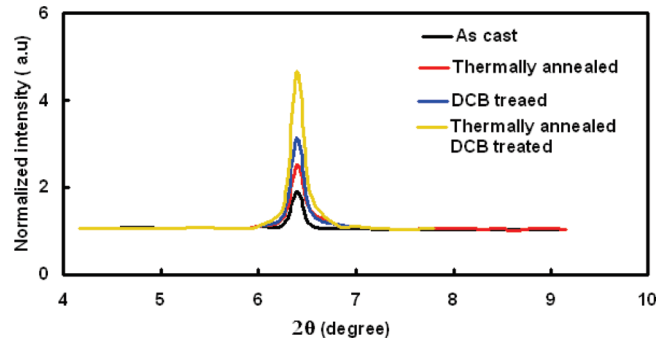

FIGURE 7. XRD pattern for copolymer P:PCBM thin films for different annealing conditions.

As seen in Figure 7, the as-cast film exhibits a peak centered at $2\theta = 6.4°$, which corresponds to the copolymer **P**:PCBM related to an interplanar distance of 8.2 ang. Annealing leads to higher peak intensity, indicating a higher degree of crystallinity. The diffraction intensity of the thermally annealed and DCB-treated blend also increases. These changes in the film crystallinity after thermal annealing agree with what is observed in the absorption spectra. Because most of the fullerene acceptors, such as PCBM, do not show any diffraction patterns in the range of 2θ values used (51), the changes in crystallinity of the blended film after thermal annealing are mainly attributed to an increase in crystalline domains of the copolymer **P** donor material. The values of the crystallite size of copolymer **P** for the as-cast, DCB-treated, and thermally annealed DCB treated **P**:PCBM blends estimated from eqs 2 and 4, are 8.5, 10.6, and 12.3 nm, respectively. The increase in the crystallite size in the **P**:PCBM blend after solvent and thermal annealing is mainly caused by the **P** chains self organization, into an ordered structure, as has been recently reported for P3HT:PCBM blend (52). The increase in the crystallinity of copolymer **P** upon DCB treatment and thermal annealing leads to an improvement in the hole mobility that increases the overall PCE.

We have also examined the effect of DCB treatment and thermal annealing on the surface structure of copolymer **P**:PCBM blends. The topographic images of the as-cast, DCB-treated, and thermally annealed DCB treated films revealed that there is significant change in the surface structure for both DCB-treated and thermally annealed DCB-treated films (see the Supporting Information). This feature also indicates that the crystallinity of copolymer **P** has increased upon thermal annealing, as was proved by the XRD patterns. This enhancement in the crystallinity results increased D−A interfacial area for photoinduced charge transfer and thereby a higher photocurrent is produced.

CONCLUSIONS

In polymer BHJ PV devices, the morphology of the photoactive layer is crucial for efficient charge separation and collection. Therefore, we have investigated the effect of DCB vapor treatment (solvent annealing) and thermal annealing on the optical morphology of a D−A phenylenevinylene copolymer **P**:PCBM blend. It was found that the

copolymer **P** chains can be self-organized into an ordered structure under the solvent annealing, resulting in enhanced absorption in visible region and hole mobility. Further thermal annealing of DCB vapor treatment (solvent annealing) can also effectively improve the phase separated networks for efficient charge separation and transport. This can be attributed to a further improvement in crystallinity of copolymer and effective activation of PCBM molecules to diffuse and aggregate into clusters for better electron transport.

Supporting Information Available: Optical topographical images of the as-cast, DCB-treated, and thermally annealed DCB treated copolymer **P**:PCBM thin films (PDF). This material is available free of charge via the Internet at http://pubs.acs.org.

REFERENCES AND NOTES

(1) Dennler, G.; Scharber, M. C.; Brabec, C. J. *Adv. Mater.* **2009**, *21*, 1323–1338.
(2) Thompson, B. C.; Frechet, J. M. J. *Angew. Chem., Int. Ed.* **2008**, *47*, 58–77.
(3) Peet, J.; Kim, J. Y.; Lee, K.; Coates, N. E.; Ma, W. L.; Moses, D.; Heeger, A. J.; Bazan, B. C. *Nat. Mater.* **2007**, *6*, 497–500.
(4) Guenes, S.; Neugebauer, H.; Sariciftci, N. S. *Chem. Rev.* **2007**, *107*, 1324–1338.
(5) Kroon, R.; Lenes, M.; Hummelen, J. C.; Blom, P. W. M.; De Boer, B. *Polym. Rev.* **2008**, *48*, 531–582.
(6) Li, G.; Shrotriya, V.; Huang, J. S.; Yao, Y.; Moriarty, T.; Emery, K.; Yang, Y. *Nat. Mater.* **2005**, *4*, 864–868.
(7) Ma, W. L.; Yang, C. Y.; Gong, X.; Lee, K. H.; Heeger, A. J. *Adv. Funct. Mater.* **2005**, *15*, 1617–1622.
(8) Yip, H.-L.; Hau, S. K.; Baek, N. S.; Ma, H.; Jen, A. K.-Y. *Adv. Mater.* **2008**, *20*, 2376–2382.
(9) Hau, S. K.; Yip, H.-L.; Ma, H.; Jen, A. K.-Y. *Appl. Phys. Lett.* **2008**, *93*, 233304/1–233304/3.
(10) Scharber, M. C.; Wuhlbacher, D.; Koppe, M.; Denk, P.; Waldauf, C.; Heeger, A. J.; Brabec, C. L. *Adv. Mater.* **2006**, *18*, 789–794.
(11) Gadisa, A.; Svensson, M.; Andersson, M. R.; Inganas, O. *Appl. Phys. Lett.* **2004**, *84*, 1609–1611.
(12) Yang, X.; Loos, J.; Veenstra, S. C.; Verhees, W. J. H.; Wienk, M. M.; Kroon, J. M.; Michels, M. A. J.; Janssen, R. A. J. *Nano Lett.* **2005**, *5*, 579–583.
(13) Mataga, N.; Chosrowjan, H.; Taniguchi, S. *J. Photochem. Photobiol.* **2005**, *6*, 37–79.
(14) Hou, J.; Park, M.; Zhang, S.; Yao, Y.; Chen, L.; Li, J.; Yang, Y. *Macromolecules* **2008**, *41*, 6012–6018.
(15) Colladet, K.; Fourier, S.; Cleij, T. J.; Lutsen, L.; Gelan, J.; Vanderzande, D.; Nguyen, L. H.; Neugebauer, H.; Sariciftci, S.; Aguirre, A.; Janssen, G.; Goovaerts, E. *Macromolecules* **2007**, *40*, 65–72.
(16) Zhang, C.; Choi, S.; Haliburton, J.; Cleveland, T.; Li, R.; Sun, S.; Ledbetter, A.; Bonner, C. E. *Macromolecules* **2006**, *39*, 4317–4326.
(17) Wang, E.; Wang, L.; Lan, L.; Luo, C.; Zhuang, W.; Peng, J.; Cao, Y. *Appl. Phys. Lett.* **2008**, *92*, 033307/1–033307/3.
(18) Blouin, N.; Michaud, A.; Gendron, D.; Wakim, S.; Blair, E.; Neagu-Plesu, R.; Belletete, M.; Durocher, G.; Tao, Y.; Leclerc, M. *J. Am. Chem. Soc.* **2008**, *130*, 732–742.
(19) Baek, N. S.; Hau, S. K.; Yip, H.-L.; Acton, O.; Chen, K.-S.; Jen, A. K.-Y. *Chem. Mater.* **2008**, *20*, 5734–5736.
(20) Hou, J. H.; Chen, H.-Y.; Zhang, S. Q.; Li, G.; Yang, Y. *J. Am. Chem. Soc.* **2008**, *130*, 16144–16145.
(21) Park, S. H.; Roy, A.; Beaupre, S.; Cho, S.; Coates, N.; Moon, J. S.; Moses, D.; Leclerc, M.; Lee, K.; Heeger, A. J. *Nat. Photonics* **2009**, *3*, 297–303.
(22) Roncali, J.; Leriche, P.; Cravino, A. *Adv. Mater.* **2007**, *19*, 2045–2060.
(23) Liang, Y. Y.; Feng, D. Q.; Wu, Y.; Tsai, S. T.; Li, G.; Ray, C.; Yu, L. P. *J. Am. Chem. Soc.* **2009**, *131*, 7792–7799.
(24) Kim, Y.; Lee, K.; Coates, N. E.; Moses, D.; Nguyen, T. Q.; Dante, M.; Heeger, A. J. *Science* **2007**, *317*, 222–225.
(25) Erb, T.; Zhokhavets, U.; Gobsch, G.; Raleva, S.; Stühn, B.; Schilinsky, P.; Waldauf, C.; Brabec, C. J. *Adv. Funct. Mater.* **2005**, *15*, 1193–1196.
(26) Zhokhavets, U.; Erb, T.; Hoppe, H.; Gobsch, G.; Sariciftci, N. S. *Thin Solid Films* **2006**, *496*, 679–682.
(27) Reyes, M. R.; Kim, K.; Carroll, D. L. *Appl. Phys. Lett.* **2005**, *87*, 083506/1–083506/3.
(28) Li, G.; Yao, Y.; Yang, H.; Shrotriya, V.; Yang, G.; Yang, Y. *Adv. Funct. Mater.* **2007**, *17*, 1636–1644.
(29) Krebs, F. C.; Jorgensen, M.; Norrman, K.; Hagemann, O.; Alstrup, J.; Nielsen, T. D.; Fyenbo, J.; Larsen, K.; Kristensen, J. *Sol. Energy Mater. Sol. Cells* **2009**, *93*, 422–441.
(30) Krebs, F. C.; Gevorgyan, S. A.; Alstrup, J. *Sol. Energy Mater. Sol. Cells* **2009**, *19*, 5442–5451.
(31) Krebs, F. C. *Sol. Energy Mater. Sol. Cells* **2009**, *93*, 394–412.
(32) Joergensen, M.; Norrman, K.; Krebs, F. C. *Sol. Energy Mater. Sol. Cells* **2008**, *92*, 686–714.
(33) Chambon, S.; Manceau, M.; Firon, M.; Cros, S.; Rivaton, A.; Gardette, J. *Polymer* **2008**, *49*, 3288–3294.
(34) Norrman, K.; Krebs, F. C. *Sol. Energy Mater. Sol. Cells* **2006**, *90*, 213–227.
(35) Kawano, K.; Pacios, R.; Poplavskyy, D.; Nelson, J.; Bradley, D. D. C.; Durrant, J. R. *Sol. Energy Mater. Sol. Cells* **2006**, *90*, 3520–3530.
(36) Krebs, F. C.; Carle, J. E.; Cruys-Bagger, N.; Andersen, M.; Lilliedal, M. R.; Hammond, M. A.; Hvidt, S. *Sol. Energy Mater. Sol. Cells* **2005**, *86*, 499–516.
(37) Jeranko, T.; Tributsch, H.; Sariciftci, N. S.; Hummelen, J. C. *Sol. Energy Mater. Sol. Cells* **2004**, *83*, 247–262.
(38) Mikroyannidis, J. A.; Sharma, S. S.; Vijay, Y. K.; Sharma, G. D. *ACS Appl. Mater. Interfaces* **2009**; DOI: 10.1021/am9006897.
(39) Brown, P. J.; Thomas, D. S.; Köhler, A.; Wilson, J. S.; Kim, J. S.; Ramsdale, C. M.; Sirringhaus, H.; Friend, R. H. *Phys. Rev. B* **2003**, *67*, 064203/1-–064203/16.
(40) Sundberg, M.; Inganäs, O.; Stafström, S.; Gustafsson, G.; Sjögren, B. *Solid State Commun.* **1989**, *71*, 435–439.
(41) Park, J. H.; Kim, J. S.; Lee, J. H.; Lee, W. H.; Cho, K. *J. Phys. Chem. C* **2009**, *113*, 17579–17584.
(42) Zhao, Y.; Xie, Z.; Qu, Y.; Geng, Y.; Wang, L. *Appl. Phys. Lett.* **2007**, *90*, 043504/1–043504/3.
(43) Schilinsky, R.; Waldauf, C.; Brabec, C. J. *Appl. Phys. Lett.* **2002**, *81*, 3885–3887.
(44) Hoppe, H.; Sariciftci, N. S. *J. Mater. Res.* **2004**, *19*, 1924–1945.
(45) Forrest, S. R. *MRS Bull.* **2005**, *30*, 28–32.
(46) Peumans, P.; Yakimov, A.; Forrest, S. R. *J. Appl. Phys.* **2003**, *93*, 3693–3723.
(47) Mihailetchi, V. D.; Xie, H.; de Boer, B.; Koster, L. J. A.; Blom, P. W. M. *Adv. Funct. Mater.* **2006**, *16*, 699–708.
(48) Koster, L. J. A.; Smits, E. C. P.; Mihailetchi, V. D.; Blom, P. W. M. *Phys. Rev. B* **2005**, *72*, 085205/1–085205/9.
(49) Mihailetchi, V. D.; Koster, L. J. A.; Hummelen, J. C.; Blom, P. W. M. *Phys. Rev. Lett.* **2004**, *93*, 216601/1–216601/4.
(50) Goodman, A. M.; Rose, A. *J. Appl. Phys.* **1971**, *42*, 2823–2830.
(51) Chikamatsu, M.; Nagamatsu, S.; Yoshida, Y.; Satio, K.; Yase, K. *Appl. Phys. Lett.* **2005**, *87*, 203504/1–203504/3.
(52) Zhao, Y.; Guo, X.; Xie, Z.; Qu, Y.; Geng, Y.; Wang, L. *J. Appl. Poly. Sci.* **2009**, *111*, 1799–1804.

AM900728F